2010 IEEE International Conference on Robotics and Automation
Anchorage Convention District
May 3-8, 2010, Anchorage, Alaska, USA

Photoelastic Stress Analysis Error Quantification in Vasculature Models for Robot Feedback Control

Carlos Tercero, Seiichi Ikeda, Motoki Matsushima and Toshio Fukuda, *Micro-nano Systems Engineering Department, Nagoya University*
Makoto Negoro, *Neurosurgery Department, Fujita Health University*
Ikuo Takahashi, *Neurosurgery Department, Anjo Kosei Hospital*

***Abstract*—Real-time and accurate stress calculation in walls of vasculature is desired to provide catheter insertion robots of feedback control without changing the catheter stiffness and lumen. This feedback source has also applications in endovascular surgery simulation for human skills and medical tools evaluation. For that purpose we consider photoelastic effect, as birefringence produced by light retardation relates with the stress inside the photoelastic materials. In this research a polariscope was designed for urethane elastomer vasculature models, the photoelastic coefficient of urethane elastomer was measured, and the camera system was calibrated to quantify and reduce error of the measurement system. An average error of 3.6% was found for the pressure range of 70-189 mmHg inside the model of urethane elastomer, this enables to calculate accurately stress in vasculature models during Human Blood Pressure Simulation (HBPS). That way we will be able to compare in a closed loop stress produced by HBPS and by the catheter motion when manipulated by a robot.**

I. Introduction

TRAINING with simulators reduces risks of injury and costs during practice for minimally invasive surgery [1].

Vascular disease is a major global cause of death [2], therefore it is necessary to develop endovascular surgery simulators. Silicone vasculature was proposed in [3] for that purpose, this simulator has silicone models of femoral, iliac, aorta, abdominal, coronaries, subclavians, carotids and cerebral arteries. It was built using a tomogram of human vasculature and recreates human arteries lumen with 13μm of accuracy. The silicone vasculature allows flow circulation and a maximum pressure of 200mmHg. Those special properties enable practicing placement of coils and stents in diseased vasculature models. The use of photoelastic effect for measuring the stress in walls of urethane vasculature was proposed in [4]. Stress in photoelastic materials produces birefringence, visible with a polariscope and resulting from the phase shift between light

Manuscript received September 15, 2009. This work was supported by JSPS and Nagoya University.

C. Tercero is with Nagoya University, Aiichi-ken Nagoya-shi Chikusa-ku Furo-cho 1, 464-8603 JAPAN (phone: +81-52-788-6013; fax: +81-52-788-6013; e-mail: tercero@robo.mein.nagoya-u.ac.jp).

S. Ikeda is with Nagoya University, Aiichi-ken Nagoya-shi Chikusa-ku Furo-cho 1, 464-8603 JAPAN (phone: +81-52-788-6013; fax: +81-52-788-6013; e-mail: ikeda @robo.mein.nagoya-u.ac.jp).

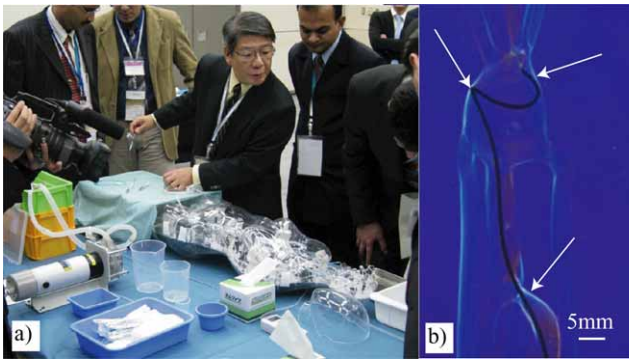

Fig. 1: a) Endovascular Surgery Simulator. b) Birefringence consequence of stress applied to the vasculature model by a guide wire.

entering and exiting photoelastic material. The phase shift is generally called retardation, here termed *Re* and measured in nanometers. The optical path length *D* is the thickness of the photoelastic material where polarized light suffers retardation. The magnitude of the principal stress component (σ_1-σ_2) is calculated with equation (1), for that the studied material photoelastic coefficient *C* should be known [5].

$$\sigma_1 - \sigma_2 = \frac{\mathrm{Re}}{CD} \tag{1}$$

In previous studies photoelastic effect was used with a catheter insertion robot to evaluate catheters [6-7] and in an augmented reality system to recreate interventional radiology environment [8], and to measure the stress produced by human blood pressure simulation inside models of vasculature for a pressure range of 87.5-152mmHg in [9]. However the photoelastic stress measurement error sources has not been quantified yet, this step is essential to develop a real time stress measurement system for vasculature models.

In this research we will present a calibration method for the transmittance equation to measure the optical path length, a polariscope designed for our simulation purpose, the deduction of the photoelastic coefficient of urethane elastomer, and the normalization parameters calibration to calculate the principal component of stress in the vasculature model with an inner pressure range of 40-189mmHg. It is desirable to measure stress with an error below 5% for the HBPS range, to use it as reference for control loop illustrated in figure 2.

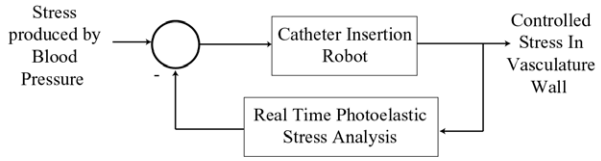

Fig 2: Desired feedback control for the catheter insertion robot.

I. Materials and Methods

A. Transmittance Equation Calibration

Transmittance of blue light was used to calculate the optical path length in multilayered models of silicone and urethane elastomer [9]. At the studied pressure ranges, the contribution of the layers of silicone elastomer to retardation and transmittance may be neglected, as silicone is transparent and urethane elastomer is dyed yellow. A urethane elastomer membrane with variable thickness was built using a stair-case shaped casting mold. The depth difference between neighbor levels of the casting mold is 0.2mm. Then an optic system with a blue filter was constructed, and an image of the model was captured to study the transmittance of blue light through the membrane. The thickness of the membrane was measured at 11 locations using a UV Laser Microscope, Figs. 3-4. The relation between transmittance and thickness was then deduced.

B. Polarizer configuration and mathematic model of retardation

As it is desirable to integrate the stress measurement system to the endovascular surgery simulator shown in figure 1, it is required to use film instead of glass for polarizer, quarter wave plates and color filters to reduce the space occupied by the optic system. Therefore the polariscope configuration should be robust against the quarter wave manufacturing accuracy, for that we propose the polariscope shown in figure 5. The normalized intensity of green light I_{GN} can be expressed with equation (2) using Jones calculus [10]:

$$I_{GN} = P_{(\pi/2)}.R_{(\lambda_{ex}/4,-\pi/4)}.R_{(\mathrm{Re},\theta)}.R_{(\lambda_{ex}/4,\pi/4)}.P_{(0)}$$

$$\Leftrightarrow I_{GN} = \sin^2\left(\frac{\mathrm{Re}\,\pi}{\lambda_G}\right)\left(\cos^2(2\theta)\sin^2\left(\frac{\lambda_{ex}\pi}{2\lambda_G}\right)+\sin^2(2\theta)\right) \quad (2)$$

Where θ is the direction of stress, $\lambda_{ex}/4 = 140$ nm is the wave length of the quarter wave plates, λ_G is the wavelength of the perceived green light, $P_{(0)}$ is the polarizer matrix, $P_{(\pi/2)}$ the analyzer matrix, $R_{(\lambda,\phi)}$ is the matrix of a retarder of λ nanometers rotated ϕ radians. In this configuration we expect λ_G to be as close as possible to λ_{ex} for reducing the system error.

C. Photoelastic Coefficient of Urethane Elastomer

In this study we used for manufacturing all models NIPOLAN5120 urethane elastomer dyed yellow with I-01-001Y of Epoch Co at 0.1w%. If we consider the urethane elastomer membrane of figure 6.a is under a tensile force F when placed inside the polariscope of figure 5 instead of the vasculature model, then the stress in the membrane may be calculated using equation (1) or (3). Therefore we are able to calculate the photoelastic coefficient of urethane elastomer using equation (4) that is independent of the membrane thickness. L is the membrane width.

$$\sigma_1 - \sigma_2 = \frac{F}{LD} \quad (3)$$

$$\Rightarrow C = \frac{\mathrm{Re}\,L}{F} \quad (4)$$

We built the device shown in figure 6.b, composed of a C-clamp used to apply gradually tension to the membrane, and coupled with a force sensor. In this figure also some of the elements of the polariscope are shown.

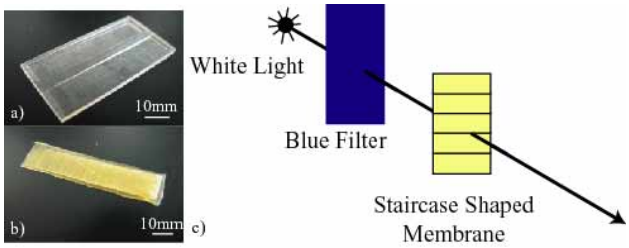

Fig.3. a) Stair case shaped casting mold. b) Variable thickness urethane elastomer membrane. c) Blue light transmittance measurement optic system.

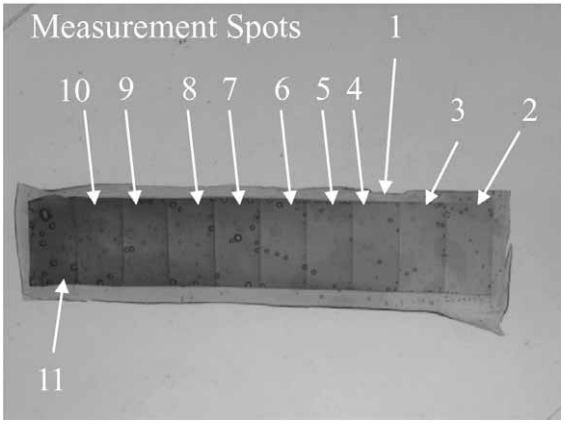

Fig.4. Locations in the variable thickness membrane where the blue light intensity and thickness were measured.

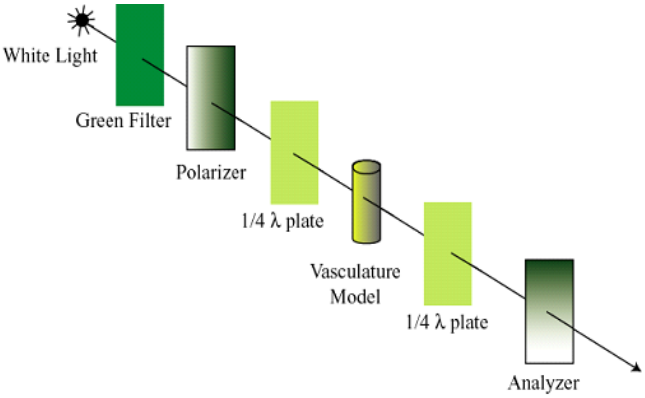

Fig.5. Polariscope configuration to reduce the effect of the quarter wave plates manufacturing precision in the error of the system.

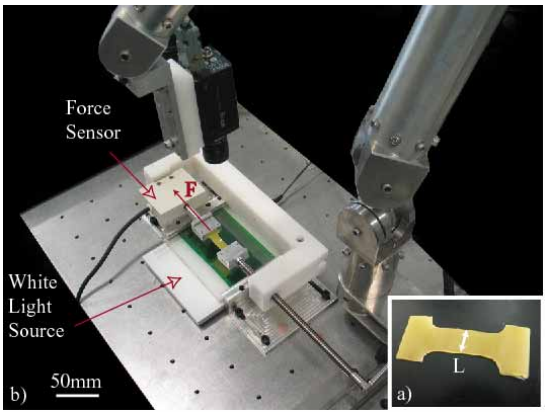

Fig.6. a) Membrane used for deducing the photoelastic coefficient of urethane elastomer. b) Variable tension device for photoelastic coefficient calculation.

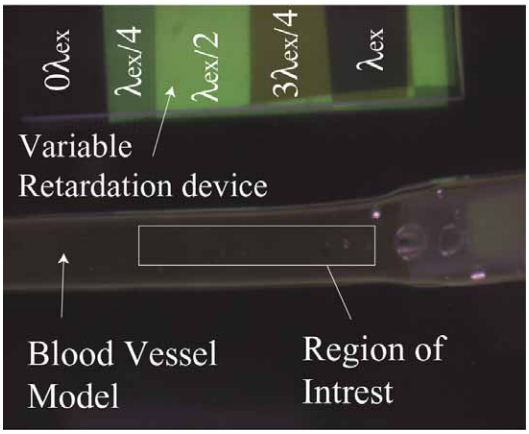

Fig.7. Image of light retardation using the polariscope with: Quarter wave plates piled in a variable retardation device used for λ_G calibration. Blood vessel model region of interest.

Tension was applied to the membrane in a range of 0.3-3.7 N, while the photoelastic images were captured. In this range the complete first fringe of retardation is visible; this ensures a proper calculation of the photoelastic coefficient. A total of 19 samples were captured obtaining simultaneous measurements of retardation *Re*, applied tension *F* and membrane with *L*.

D. Camera calibration

For capturing the photoelastic images an 8bit RGB camera was used. To calculate the optical path length the blue light wave length is not a parameter of interest, meanwhile to calculate the *Re* green light wave length λ_G is essential. The green filter reduces the effect of red and blue light in the green channel of the camera. λ_G is the principal wavelength value captured by the camera's green channel, and changes with the environment illumination and lens configuration. Therefore we propose the device showed in figure 7 to calibrate this parameter before measuring the retardation.

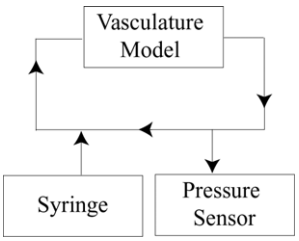

Fig.8. Fluid closed loop for pressure variation and measurement inside the blood vessel model.

In this device, four wave plates of 140nm of different sizes are piled providing 5 zones with retardations of $0\lambda_{ex}$, $\lambda_{ex}/4$, $\lambda_{ex}/2$, $3\lambda_{ex}/4$ and λ_{ex}=560nm. When this device is placed in the polariscope with an angle of $\pi/2$, equation (2) is simplified to equation (5). As *Re* is known for each zone of the device and the normalized value of green of a studied area I_{GN} can be deduced from equation (6) then the value of λ_G may be calculated.

$$I_{GN} = \sin^2 \frac{\pi}{\lambda_G} \mathrm{Re} \tag{5}$$

$$I_{GN} = \frac{I_G - I_{G0\lambda ex}}{I_{G\lambda ex/2} - I_{G0\lambda ex}} \tag{6}$$

I_G is the average green value of any studied region in figure 7, $I_{G0\lambda ex}$ is considered the minimum value of green as there is noretardation in $0\lambda_{ex}$, $I_{G\lambda ex/2}$ is considered the maximum value of green as (5) should maximize near this point.

E. Photoelastic Stress Analysis Error Quantification

The blood vessel model as shown in figure 7 is placed in the polariscope inside a glycerin bath. When pressure *P* inside the model is above 40mmHg, the shape of the model may be approximated to a cylinder of radius *r* and wall thickness *D*. Then the model wall stress is calculated using equation (7), those results are used as reference to quantify the error introduced by the photoelastic measurement system using equations (1-2).

$$\sigma_1 - \sigma_2 = \frac{rP}{D}\left(\frac{r-2D}{2r-D}\right) \tag{7}$$

For a range from 40-189mmHg stress will be calculated using both methods for 16 samples. *P* is increased using a syringe and measured using a sensor for measuring pressure below 200mmHg, both connected to the blood vessel model as illustrated in figure 8. Values of green were measured in the region of interest (ROI) for each sample. The average green value ROI for a pressure *P* is called I_{GP}; this value should be normalized using equation (8).

$$I_{GNP} = \frac{I_{GP} - I_{GMin}}{I_{GMax} - I_{GMin}} \tag{8}$$

The minimum and maximum value of green I_{GMin}, I_{GMax} are obtained by setting *P* at 40mmHg and above 200mmHg. Then the limit values are calculated using equations (9) and (10),

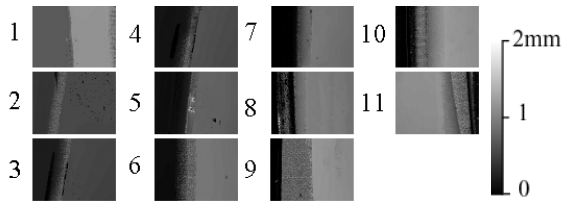

Fig.9 Location 1 shows the depth difference between the base plate and the border of the membrane. Locations 2-11 show the difference between the border of the membrane and the level of the stair case shape. Measurements were done at the 11 locations using a UV laser microscope.

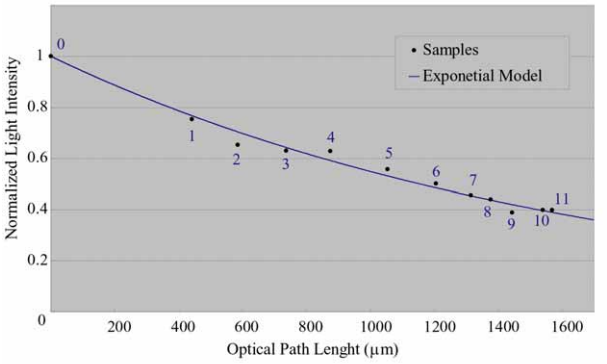

Fig.10: Plot of relation between blue light transmittance and membrane thickness. Locations names are shown in blue numbers; location 0 is the measured directly from the filter.

σ_{IG40} and σ_{IG200+} are the standard deviation of I_{G40} and I_{G200+}.

$$I_{GMin} = I_{G40} - \sigma_{IG40} \quad (9)$$

$$I_{GMax} = I_{G200+} + \sigma_{IG200+} \quad (10)$$

II. Results

A. Transmittance Equation Calibration

The results of measurements done with the UV laser microscope are shown in figure 9, and plotted against the values of blue light transmittance in figure 10. The obtained exponential approximation of the relation between them is shown in equation (11), with a transmittance coefficient T_c=1666.66 and a correlation coefficient of R=0.982. I_B is the light blue intensity at the studied location, I_{BMax} =132.08 is the average blue light intensity in the area where there is no membrane covering the filter. The normalization of I_B by I_{BMax} gives robustness to equation (11)

$$D = -T_c \ln(I_B / I_{BMax}) \quad (11)$$

B. Camera calibration

The normalized values of green were plotted against their corresponding retardation in figure 11. The value of λ_G is obtained by minimizing the error between the plot and the model of equation (5). The error is minimized when λ_G=510 in (5). With this value equation (2) simplifies to equation (12).

$$I_{GNP} = \sin^2\left(\frac{\mathrm{Re}\,\pi}{\lambda_G}\right)\left(0.976 + 0.024\sin^2(2\theta)\right) \quad (12)$$

Equation (12) will be approximated in this case to (13), by suppressing the contribution made by the direction of stress as it maximizes in 2.4%.

$$I_{GNP} = \sin^2\left(\frac{\mathrm{Re}\,\pi}{\lambda_G}\right) \quad (13)$$

C. Photoelastic Coefficient of Urethane Elastomer

For this experiment λ_G was found to be 521 nm, figure 12 shows the plot of the variation of the normalized green light intensity with applied force, showing that complete first fringe was captured. Figure 13 shows the value of the photoelastic coefficient obtained for each sample, the average value of them is $1.284 \times 10^{-9} Pa^{-1}$.

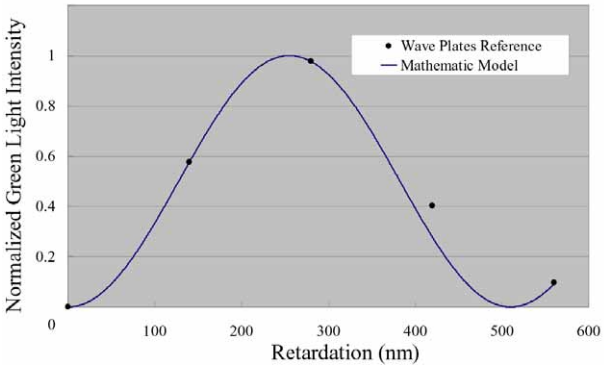

Fig.11: Plot of the retardation introduced by the quarter plates in the studied areas and their respective normalized green light intensity. In

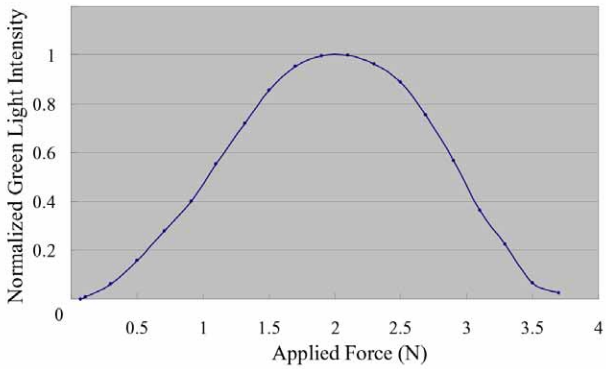

Fig.12: Variation of the green light intensity with the applied force.

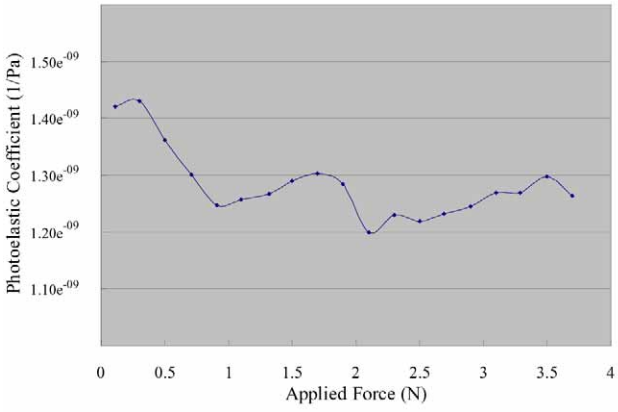

Fig 13: Variation of the photoelastic coefficient with the applied force for the 19 samples

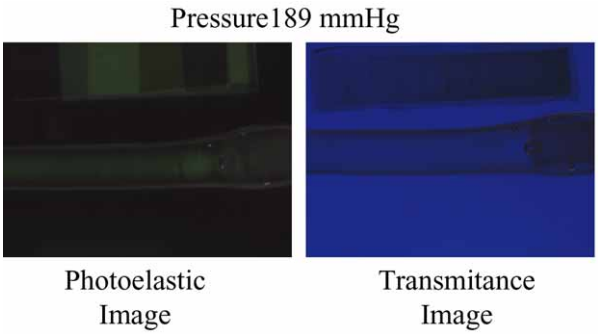

Fig.14: Source image example for retardation (left), and for optical path length calculation (right).

D. Photoelastic Stress Analysis Error Quantification

A sample of source images of photoelasticity and transmittance measurements is shown in figure 14. We deduced from I_{G40} that I_{GMin} is 23.32 and from I_{G200+} that I_{GMax} is 53.86. For this experiment the value of λ_G was obtained from the results shown on figure 11. The optical path length was calculated by applying equation (11) to the transmittance images set. The resulting set is shown in figure 15; a threshold of 200μm was applied to eliminate image noise, enhancing the borders of both urethane objects. Stress measurements were performed for the different values of P in the ROI of the photoelasticity source images. First using the photoelastic stress analysis (1, 11, and 13) and then by equations (7, 11). In this case as $r>>D$, therefore the influence of the wall thickness in the final result is almost the same for both methodologies, then the stress measured using equations (7,11) may be used as reference for the photoelastic error quantification. The results for both methods are plotted in figure 16. The difference between both methods is shown in figure 17; an average error of 3.6% is present for pressure above 70mmHg. Error is large for pressure ranges below 70mmHg.

Finally the photoelastic stress analysis was applied by separate to every pixel of the complete region corresponding to blood vessel model of the photoelasticity source images. The corresponding result set of stress images is shown on figure 15. We can perceive that an amount of pixels is blacked out in some parts of the stress images corresponding to the pressure range below 70mmHg. This means that those pixels where below the value defined for I_{GMin}.

III. Discussion

As pressure increases inside the model the optical path length reduces in the corresponding set of images of figure 15. Also the characteristics of the variable thickness membrane are visible in that figure, confirming the plot of figure 10. The photoelastic coefficient C was determined to be $1.28e^{-9}$, this differs from the value deduced in [11]. Therefore we may assume that the value of T_c and C are valid only for the NIPOLAN5120 urethane elastomer dyed yellow with I-01-001Y of Epoch Co at 0.1w%. In previous studies polariscopes with more sensibility to the stress direction were used [3, 4, 6, 9 and 11]. For those designs high precision wave plates and quarter wave plates are necessary to obtain more accuracy in measurements of stress magnitude and direction. To ensure accuracy in the measurements, the calibration procedure should be repeated before start measuring the samples. Another option may be isolate in a dark space the camera, polariscope and model.

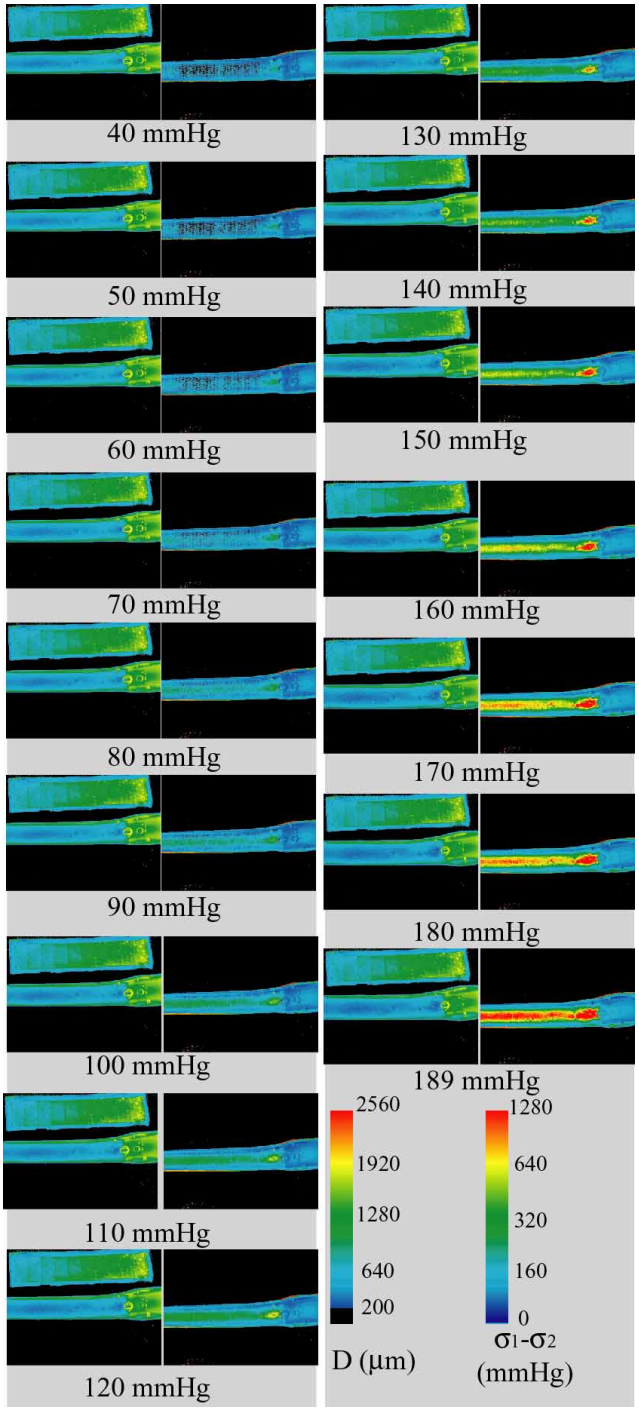

Fig.15: Result image of the 16 samples, below each set of 2 images the corresponding pressure is written. For each set, optical path length D is left and the corresponding photoelastic stress analysis is right. The variable thickness membrane appears in all the optical path length images.

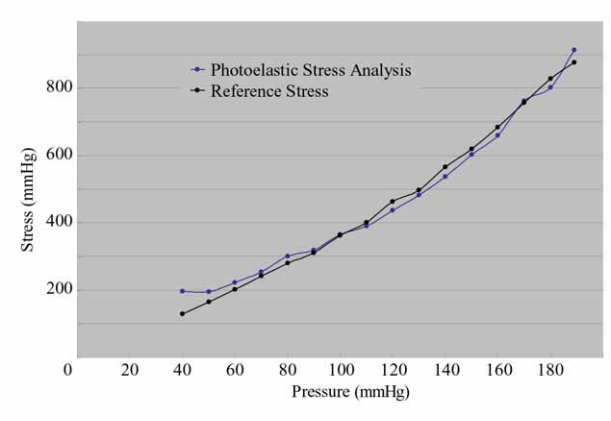

Fig. 16: Stress in the model wall variation against pressure inside the model, calculated using photoelastic stress analysis and model radius variation that is used as reference.

Force sensors placed on the catheter tip [12] are complementary to the photoelastic stress analysis as they modify the stiffness and lumen of medical catheters. Therefore the range of tools that may be evaluated using force sensors is limited to modified catheters. In future with photoelastic stress analysis, feedback control may be provided to the catheter insertion robot when manipulating any kind of catheters, guide wire, stents or coils, Fig. 18.We can perceive in the stress images, especially for pressure ranges above 150 mmHg, that as we move away from the axis of the model stress value decreases gradually. This happens because of changes in the orientation of the crystals forming the urethane elastomer membrane as we move along the curvature of the model's cylindrical shape. For that error a correction method could be applied as we move away from the axis of the blood vessel. But for that image processing software must be developed for finding the axis orientation and borders of the model.

IV. Conclusion

Human blood pressure varies in the range of 50 -152 mmHg [13-14], and was simulated in [9] for a range of 87.5-152.5 mmHg with 5.6% of error. A calibration methodology was proposed to deduce the more appropriate values for the parameters C, T_c, I_{GMin}, I_{GMax}, λ_G, and I_{BMax} for photoelastic stress analysis. The calibration showed an average error of 3.6% in the range of 70-189mmHg, and large error for pressures below 70mmHg. Therefore with this calibration methodology principal component of stress in the vasculature wall may be calculated accurately for human blood pressure simulation. From them the normal range of stress in blood vessel model may be deduced and then used as reference for the catheter insertion robot feedback control as shown in figure 2. As remaining error sources we have the difference between perceived light λ_G and λ_{ex}, manufacturing accuracy of quarter wave plates, the simplification of equation (2) and changes in the orientation of the crystals of the urethane membrane.

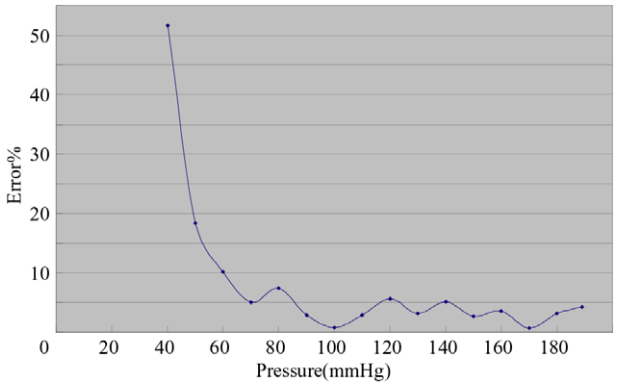

Fig.17: Variation of error of photoelastic stress analysis with pressure changes inside the vasculature model.

References

[1] K. Kunkler, "The role of Medical simulation: an overview," International *Journal of Medical Robotics and Computer Assisted Surgery*, vol.2, pp.203-210, 2006.

[2] C. Murray, A. Lopez, "Alternative projections of mortality and disability by cause 1990–2020: Global Burden of Disease Study" *The Lancet*, Vol. 349, pp. 1498-1504, 1997.

[3] S. Ikeda, F. Arai, T. Fukuda, M. Negoro, K. Irie, "An in vitro patientspecific biological model of the cerebral artery reproduced with a membranous configuration for simulating endovascular intervention," *J Robotics and Mechatronics*, vol. 17, no. 3, pp. 327–333, 2005.

[4] S. Ikeda, T. Fukuda, F. Arai, et al., "Patient-specific neurovascular simulator for evaluating the performance of medical robots and instruments," in *Proc. of the IEEE-ICRA*, 2006, pp. 625-630.

[5] A. Kuske G. Robertson, "Photoelastic Stress Analysis", A Wiley-Interscience Publication, (1974), pp. 87-109, 263-274

[6] C. Tercero, Y. Okada, S. Ikeda, T. Fukuda, K. Sekiyama, M. Negoro, I. Takahashi. "Numerical evaluation method for catheter prototypes using photo-elastic stress analysis on patient-specific vascular model," *International Journal of Medical Robotics and Computer Assisted Surgery,* Vol.3:4 pp. 349-354, 2007.

[7] C. Tercero, S. Ikeda, T. Uchiyama, T. Fukuda, F. Arai, Y. Okada, Y. Ono, R. Hattori, T. Yamamoto, M. Negoro, I. Takahashi. "Autonomous Catheter Insertion System using Magnetic Motion Capture Sensor for endovascular surgery," *International Journal of Medical Robotics and Computer Assisted Surgery*. Vol. 3:1 pp 52-58, 2007.

[8] S. Ikeda, C. Tercero, T. Fukuda, Y. Okada, F. Arai, M. Negoro, M. Hayakawa, I. Takahashi. "Patient-Specific IVR Endovascular Simulator with Augmented Reality for Medical Training and Robot Evaluation," *Journal of Robotics and Mechatronics*. Vol.20, No.3, pp. 441-448, 2008.

[9] C. Tercero, S. Ikeda, E. Tijerino, M. Matsushima, T. Fukuda, M. Negoro, I. Takahashi. "Human Blood Pressure Simulation for Stress Analysis in Model of Vasculature using Photoelastic Effect" International Journal of Automation Technology. Vol.3 :5, 2009, in press.

[10] D. Goldstein. "Polarized Light" Marcel Dekker, Inc. Ch11 pp.211-239.

[11] Y. Okada, S. Ikeda, T. Fukuda, F. Arai, M. Negoro, I. Takahashi, "Photoelastic Stress Analysis on Patient-Specific Anatomical Model of Cerebral Artery", in *Proc. of the International Symposium on Micro-NanoMechatronics and Human Science*,2007, pp. 538-543.

[12] M. Tanimoto, F. Arai, T. Fukuda, H. Iwata, K. Gotoh, M. Hashimoto and M. Negoro, "Study on Micro Force Sensor for Minimum Invasive Surgery," Trans. of the Japan Soc. of Mech. Eng., C 64-620, JSME, pp150-155, 1998.

[13] J. Panza, "High-Normal Blood Pressure more "High" than "Normal"," *N Engl J Med*, vol. 345, no. 18, pp.1337-1340, 2001.

[14] B. De Bruyne, J. Bartunek, S.K. Sys, et al., "Simultaneous coronary pressure and flow velocity measurements in humans," *Circulation*, vol. 94, pp.1842-1849, 1996.